

# Interplay of Coulomb and electron-phonon interactions in graphene

D. M. Basko<sup>1,\*</sup> and I. L. Aleiner<sup>2</sup>

<sup>1</sup>*International School of Advanced Studies (SISSA), via Beirut 2-4, 34014 Trieste, Italy*

<sup>2</sup>*Physics Department, Columbia University, New York, NY 10027, USA*

We consider mutual effect of the electron-phonon and strong Coulomb interactions on each other by summing up leading logarithmic corrections via the renormalization group approach. We find that the Coulomb interaction enhances electron coupling to the intervalley  $A_1$  optical phonons, but not to the intravalley  $E_2$  phonons.

*Introduction.*— Electron-phonon coupling (EPC) in graphene is currently a subject of intense research. Experimental information on EPC is obtained by Raman spectroscopy [1, 2, 3, 4, 5] and angle-resolved photoemission spectroscopy (ARPES) [6]. Theoretically, EPC constants are usually calculated from density-functional theory (DFT) [7, 8, 9], where the exchange (Fock) term is treated in the local density approximation (LDA) [10], or the generalized gradient approximation (GGA) [11]. Disagreement between the calculated EPC and the ARPES data has been pointed out in Ref. [8].

Also, the ratio between calculated EPC constants for different phonon modes disagrees with the ratio of the integrated intensities  $I_{D^*}/I_{G^*}$  of the corresponding two-phonon Raman peaks, as noted in Ref. [12]. Namely, in the Raman spectrum of graphene two two-phonon peaks are seen: the so-called  $D^*$  peak near  $2\omega_{A_1} = 2650 \text{ cm}^{-1}$ , and the  $G^*$  peak near  $2\omega_{E_2} = 3250 \text{ cm}^{-1}$ , corresponding to scalar  $A_1$  phonons from the vicinity of the  $K$  point of the first Brillouin zone, and to pseudovector  $E_2$  phonons from the vicinity of the  $\Gamma$  point, respectively. Experimentally,  $I_{D^*}/I_{G^*} \approx 20$  [1], which cannot be reproduced with the EPC constants obtained from DFT calculations.

In this work we consider mutual effect of weak electron-phonon and strong Coulomb interactions on each other by summing up leading logarithmic corrections via the renormalization group (RG) approach, which goes beyond Hartree-Fock approximation. Coulomb interaction has been known to be a source of logarithmic renormalizations for Dirac fermions [13, 14, 15]. Coulomb renormalizations in graphene subject to a magnetic field have been considered in Ref. [16], Coulomb effect on static disorder has been studied in Refs. [17, 18, 19]. To the best of our knowledge, Coulomb renormalization of EPC has never been considered; moreover, at energies higher than the optical phonon frequency, EPC itself is a source of logarithmic renormalizations, and has to be included in the RG procedure.

Upon solution of the RG equations we obtain that (i) EPC tends to enhance Coulomb interaction, but not sufficiently to dominate over the flow to weak coupling, found earlier [15]; (ii) Coulomb interaction enhances the EPC only for the scalar  $A_1$  phonons, while renormalization of the coupling to the pseudovector  $E_2$  phonons is only due to EPC and is relatively weak, in agreement

$C_{6v}$	$E$	$C_2$	$2C_3$	$2C_6$	$\sigma_{a,b,c}$	$\sigma'_{a,b,c}$
$A_1$	1	1	1	1	1	1
$A_2$	1	1	1	1	-1	-1
$B_2$	1	-1	1	-1	1	-1
$B_1$	1	-1	1	-1	-1	1
$E_1$	2	-2	-1	1	0	0
$E_2$	2	2	-1	-1	0	0

TABLE I: Irreducible representations of the group  $C_{6v}$  and their characters.

irrep	$A_1$	$B_1$	$A_2$	$B_2$	$E_1$	$E_2$
valley-diagonal matrices						
matrix	$\mathbb{1}$	$\Lambda_z$	$\Sigma_z$	$\Lambda_z \Sigma_z$	$\Sigma_x, \Sigma_y$	$-\Lambda_z \Sigma_y, \Lambda_z \Sigma_x$
valley-off-diagonal matrices						
matrix	$\Lambda_x \Sigma_z$	$\Lambda_y \Sigma_z$	$\Lambda_x$	$\Lambda_y$	$\Lambda_x \Sigma_y, -\Lambda_x \Sigma_x$	$\Lambda_y \Sigma_x, \Lambda_y \Sigma_y$

TABLE II: Classification of  $4 \times 4$  hermitian matrices according to irreducible representations of the  $C_{6v}$  group. Matrices joined by braces transform through each other under translations.

with the Raman data [1].

*Model.*— We measure the single-electron energies from the Fermi level of the undoped (half-filled) graphene. The Fermi surface of undoped graphene consists of two points, called  $K$  and  $K'$ . Graphene unit cell contains two atoms, each of them has one  $\pi$ -orbital, so there are two electronic states for each point of the first Brillouin zone (we disregard the electron spin). Thus, there are exactly four electronic states with zero energy. An arbitrary linear combination of them is represented by a 4-component column vector  $\psi$ . States with low energy are obtained by including a smooth position dependence  $\psi(\mathbf{r})$ ,  $\mathbf{r} \equiv (x, y)$ . The low-energy hamiltonian has the Dirac form [20]:

$$\hat{H}_{el} = \int d^2\mathbf{r} \psi^\dagger(\mathbf{r}) (-iv\mathbf{\Sigma} \cdot \nabla) \psi(\mathbf{r}). \quad (1)$$

We prefer not to give the explicit form of the isospin matrices  $\mathbf{\Sigma} \equiv (\Sigma_x, \Sigma_y)$ , which depends on the choice of basis (specific arrangement of the components in the column  $\psi$ ). We only note that all 16 generators of the  $SU(4)$  group, forming the basis in the space of  $4 \times 4$  hermitian

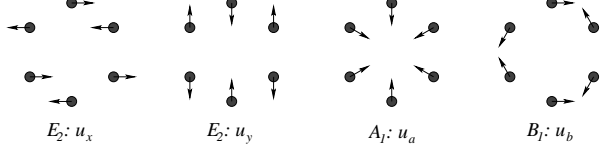


FIG. 1: Phonon displacements for  $E_2$ ,  $A_1$ , and  $B_1$  modes.

matrices, can be classified according to the irreducible representations of  $C_{6v}$ , the point group of the graphene crystal (Tables I and II). They can be represented as products of two mutually commuting algebras of Pauli matrices  $\Sigma_x, \Sigma_y, \Sigma_z$  and  $\Lambda_x, \Lambda_y, \Lambda_z$  [21, 22], which fixes their algebraic relations. By definition,  $\Sigma_x, \Sigma_y$  are the matrices, diagonal in the  $K, K'$  subspace, and transforming according to the  $E_1$  representation of  $C_{6v}$ . The Fermi velocity  $v \approx 10^8$  cm/s.

The hamiltonian of the long-range Coulomb interaction between electrons has the form

$$\hat{H}_{ee} = \frac{e^2}{2} \int d^2\mathbf{r} d^2\mathbf{r}' \frac{\hat{\rho}(\mathbf{r})\hat{\rho}(\mathbf{r}')}{|\mathbf{r} - \mathbf{r}'|}, \quad \hat{\rho}(\mathbf{r}) = \frac{\mathcal{N}}{2} \hat{\psi}^\dagger(\mathbf{r})\hat{\psi}(\mathbf{r}). \quad (2)$$

Here  $\mathcal{N}/2 = 2$  is the spin degeneracy. The background dielectric constant of the substrate is incorporated into  $e^2$ .

For low-energy electronic states EPC is efficient if the phonon wave vector is close to  $\Gamma, K$  or  $K'$  point. Considering only in-plane displacements, we have 4 degrees of freedom per unit cell. Consider the  $\Gamma$  point first. Two modes are acoustic, they weakly couple to electrons, and are neglected. The other two correspond to  $E_2$  (pseudovector) optical phonons, shown in Fig. 1. They couple to the electronic motion via the  $KK'$ -diagonal  $E_2$  matrices from Table II. The  $K$  and  $K'$  points are related by the time reversal symmetry, so the phonon frequencies are the same, and one can form real linear combinations of the modes from  $K$  and  $K'$ . They transform according to  $A_1, B_1, A_2, B_2, E_1, E_2$  representations of  $C_{6v}$ , and couple to the electronic motion via corresponding  $KK'$ -off-diagonal matrices. Linear coupling to  $A_2$  and  $B_2$  displacements is forbidden by time-reversal symmetry, and coupling to the  $E_1, E_2$  modes is numerically small [23]. The reason for this smallness is that  $E_1, E_2$  displacements do not change any C-C bond length; in the tight-binding approximation this coupling simply vanishes. Thus, we restrict our attention to the  $E_2$  modes from the  $\Gamma$  point and  $A_1$  and  $B_1$  combinations of the modes from the  $K, K'$  points, shown in Fig. 1. They are the only modes seen in the Raman spectra of graphene [1, 2, 3, 4, 5].

We take the magnitude of the carbon atom displacement as the normal coordinate for each mode, denoted by  $u_\mu$ ,  $\mu = x, y, a, b$  for the four modes, shown in Fig. 1, respectively. Upon quantization of the phonon field,  $\hat{u}_\mu$  and the phonon hamiltonian  $\hat{H}_{ph}$  are expressed in terms

$$\begin{aligned} \overleftarrow{\text{p}, \epsilon} &= -\frac{i\epsilon + v\mathbf{p} \cdot \boldsymbol{\Sigma}}{(i\epsilon)^2 - (vp)^2} & \overleftarrow{\text{q}, \omega, \mu} &= -\frac{2\omega_\mu}{(i\omega)^2 - \omega_\mu^2} \\ \overleftarrow{\text{I}} &= -\frac{3F_\mu (\Lambda\Sigma)_\mu}{\sqrt{2NM}\omega_\mu} & \overleftarrow{\text{q}, \omega} &= -\frac{2\pi e^2}{q} \end{aligned}$$

FIG. 2: Analytical expressions of the diagrammatic technique.

$$\begin{aligned} -\Sigma(\mathbf{p}, i\epsilon) &= \text{[Diagram: wavy line with arrow]} + \text{[Diagram: dashed line with arrow]} \\ -V(\mathbf{q}, i\omega) &= \text{[Diagram: wavy line]} = \text{[Diagram: wavy line]} + \text{[Diagram: wavy line with loop]} \end{aligned}$$

FIG. 3: Electron self-energy due to the screened Coulomb interaction and the EPC.

of the creation and annihilation operators  $\hat{b}_{\mathbf{q}\mu}^\dagger, \hat{b}_{\mathbf{q}\mu}$ , as

$$\hat{u}_\mu(\mathbf{r}) = \sum_{\mathbf{q}} \frac{\hat{b}_{\mathbf{q}\mu} e^{i\mathbf{q}\mathbf{r}} + \text{h.c.}}{\sqrt{2NM}\omega_\mu}, \quad \hat{H}_{ph} = \sum_{\mathbf{q}, \mu} \omega_\mu \hat{b}_{\mathbf{q}\mu}^\dagger \hat{b}_{\mathbf{q}\mu}. \quad (3)$$

The crystal is assumed to have the area  $L_x L_y$ , and to contain  $N$  carbon atoms of mass  $M$ . The  $\mathbf{q}$  summation is performed as  $\sum_{\mathbf{q}} \rightarrow L_x L_y \int d^2\mathbf{q}/(2\pi)^2$ . ‘‘h.c.’’ stands for hermitian conjugate. The two degenerate  $E_2$  modes have the frequency  $\omega_{E_2} \approx 0.196$  eV. As the  $A_1$  and  $B_1$  modes represent real linear combinations of modes from  $K, K'$  points, they have the same frequency,  $\omega_{A_1} \approx 0.170$  eV, and appear with the same coupling constant in the EPC hamiltonian:

$$\begin{aligned} \hat{H}_{EPC} &= \int d^2\mathbf{r} \hat{\psi}^\dagger(\mathbf{r}) \left[ \sum_{\mu} F_{\mu} \hat{u}_{\mu}(\mathbf{r}) (\Lambda\Sigma)_{\mu} \right] \hat{\psi}(\mathbf{r}) = \\ &= \int d^2\mathbf{r} \hat{\psi}^\dagger(\mathbf{r}) \{ F_{E_2} [\hat{u}_x(\mathbf{r})\Lambda_z\Sigma_y - \hat{u}_y(\mathbf{r})\Lambda_z\Sigma_x] + \\ &\quad + F_{A_1} [\hat{u}_a(\mathbf{r})\Lambda_x\Sigma_z + \hat{u}_b(\mathbf{r})\Lambda_y\Sigma_z] \} \hat{\psi}(\mathbf{r}). \quad (4) \end{aligned}$$

The coupling constants  $F_{E_2}$  and  $F_{A_1}$  are not related by any symmetry. However, in the tight-binding model  $F_{E_2} = F_{A_1} = 3(\partial t_0/\partial a)$ , where  $t_0$  is the nearest-neighbor coupling matrix element, and  $a$  is the bond length.

*Logarithmic self-energies.*— As we are interested in energies much higher than the temperature  $T$ , we set  $T = 0$ ; still, calculations are much more transparent in the Matsubara representation. Electron and phonon Green’s functions are given by

$$G(\mathbf{p}, i\epsilon) = -\frac{i\epsilon + v\mathbf{p}\boldsymbol{\Sigma}}{\epsilon^2 + (vp)^2}, \quad D_{\mu}(i\omega) = -\frac{2\omega_{\mu}}{\omega^2 + \omega_{\mu}^2}, \quad (5)$$

their graphical representation is shown in Fig. 2. The electronic self-energy is a sum of the Coulomb [15] and EPC [24] contributions:  $\Sigma = \Sigma^{ee} + \Sigma^{ph}$ , shown in Fig. 3.

The leading logarithmic term in  $\Sigma^{ee}$  is given by:

$$\begin{aligned} \Sigma^{ee}(\mathbf{p}, i\epsilon) &= - \int \frac{d\omega}{2\pi} \frac{d^2\mathbf{q}}{(2\pi)^2} V(\mathbf{q}, i\omega) G(\mathbf{p} - \mathbf{q}, i\epsilon - i\omega) \\ &\approx \frac{8}{\pi^2 \mathcal{N}} \left[ f(g)(2i\epsilon - v\mathbf{p}\Sigma) - \tilde{f}(g)(i\epsilon - v\mathbf{p}\Sigma) \right] \ln \frac{\xi_{max}}{\xi_{min}}, \end{aligned} \quad (6)$$

$$f(g) = 1 - \frac{\pi}{2g} + \frac{\arccos g}{g\sqrt{1-g^2}}, \quad \tilde{f}(g) = \frac{g \arccos g}{\sqrt{1-g^2}}, \quad (7)$$

$$V(\mathbf{q}, i\omega) = \frac{16g v}{\mathcal{N}} \frac{q}{q} \frac{\sqrt{(vq)^2 + \omega^2}}{gvq + \sqrt{(vq)^2 + \omega^2}}, \quad g = \frac{\pi \mathcal{N} e^2}{8v} \quad (8)$$

The lower cutoff  $\xi_{min} \sim \max\{vp, \epsilon\}$ , the upper cutoff  $\xi_{max} \sim v/a$  is of the order of the electronic bandwidth. The random phase approximation (RPA) for  $V(\mathbf{q}, i\omega)$ , shown in Fig. 3, corresponds to the leading order in the parameter  $1/\mathcal{N} = 0.25$ , assumed to be small. This assumption is better justified than the expansion in the dimensionless coupling constant  $g$ . Indeed, for  $\mathcal{N} = 4$  we have  $g = (\pi/2)(e^2/v) \approx 3.4$ ; taking into account the background dielectric screening reduces it to  $g \sim 1$ . The logarithmic divergence in the Fock self-energy  $\Sigma^{ee}$  is due to long-distance nature of the Coulomb interaction, and thus is not picked up by local approximations such as LDA or GGA.

The leading logarithmic asymptotics of  $\Sigma^{ph}$  is given by

$$\begin{aligned} \Sigma^{ph}(i\epsilon) &= - \int \frac{d\omega}{2\pi} \frac{d^2\mathbf{q}}{(2\pi)^2} \sum_{\mu} \frac{9F_{\mu}^2}{M\omega_{\mu}} \frac{\sqrt{27}a^2}{4} D_{\mu}(i\omega) \times \\ &\quad \times (\Lambda\Sigma)_{\mu} G(\mathbf{p} - \mathbf{q}, i\epsilon - i\omega) (\Lambda\Sigma)_{\mu} \approx \\ &\approx \frac{\lambda_{E_2} + \lambda_{A_1}}{2\pi} i\epsilon \ln \frac{\xi_{max}}{\xi_{min}}, \quad \lambda_{\mu} = \frac{F_{\mu}^2}{M\omega_{\mu} v^2} \frac{\sqrt{27}a^2}{4}. \end{aligned} \quad (9)$$

Here  $\xi_{min} \sim \max\{\epsilon, \omega_{\mu}\}$ ,  $\xi_{max} \sim v/a$ , and  $\sqrt{27}a^2/4$  is the area per carbon atom. The dimensionless constants  $\lambda_{E_2}, \lambda_{A_1}$  will be treated as small parameters.

The latter statement deserves some discussion. In principle, one could proceed analogously to the Coulomb case: instead of doing the perturbative expansion in  $\lambda_{\mu}$ , one could dress the bare phonon propagators by the appropriate polarization operators  $\Pi(\mathbf{q}, i\omega)$ , corresponding to  $1/\mathcal{N}$  expansion. Since  $\Pi(\mathbf{q}, i\omega) \propto q$  at large  $q$ , the dressed phonon frequency would grow as  $\sqrt{q}$ , and  $\Sigma^{ph}$  would no longer diverge logarithmically. However, the inelastic X-ray scattering data for the phonon dispersion [25] show that the phonon dispersion is smaller than the phonon frequency itself. Thus, the renormalization of the phonon frequency remains small even at  $q \sim 1/a$ , so the perturbative expansion in  $\lambda_{\mu}$  is more justified.

The logarithmically divergent integrals in Eqs. (6) and (9) have different structure due to different form of the screened interaction  $V(\mathbf{q}, i\omega)$  and the phonon propagator  $D_{\mu}(i\omega)$ . In Eq. (6) the integral is dominated by the frequencies  $|\omega| \sim vq$ , while in Eq. (9) it is  $|\omega| \sim \omega_{\mu}$ , since  $D_{\mu}(i\omega) \propto 1/\omega^2$  at  $|\omega| \gg \omega_{\mu}$ . Thus, in the calculation of

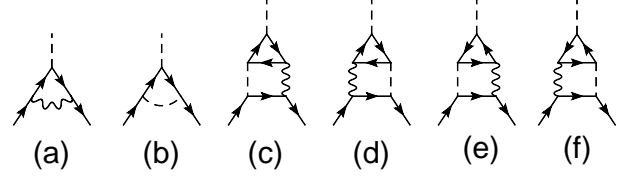


FIG. 4: Logarithmic corrections to the EPC vertex  $F_{\mu}$  of the order  $O(1/\mathcal{N}, \lambda_{\mu}^2)$ . Diagrams (c)–(f) vanish.

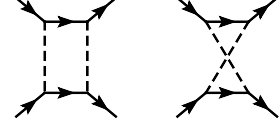


FIG. 5: Logarithmic diagrams of the order  $O(\lambda_{\mu}^2)$  not reduced to a renormalization of the EPC vertex  $F_{\mu}$ .

the leading logarithmic asymptotics it is sufficient to approximate  $D_{\mu}(i\omega) \approx -2\pi\delta(\omega)$ . This substitution makes the phonon propagator (combined with EPC vertices) formally analogous to the correlator of static disorder potential (i. e., from the point of view of electrons with  $\epsilon \gg \omega_{\mu}$  the lattice is effectively frozen). Thus, renormalizations due to EPC at  $\epsilon \gg \omega_{\mu}$  are equivalent to those due to static disorder [17, 18, 19, 22]. This equivalence holds only in the leading order in EPC, since in higher orders the phonon propagator is dressed by polarization loops, and the static disorder correlator is not.

*Renormalization group.*— The leading logarithmic terms of the perturbation theory can be collected by the RG procedure. Let us introduce the running cutoff  $\xi_{max}e^{-\ell}$ . One RG step consists of reducing the cutoff,  $\ell \rightarrow \ell + \delta\ell$ , so that  $e^{-\delta\ell} \ll 1$ , while  $(1/\mathcal{N})\delta\ell \ll 1$ ,  $\lambda_{\mu}\delta\ell \ll 1$ . The inverse Green's function transforms as

$$i\epsilon - v\mathbf{p}\Sigma - \Sigma(\mathbf{p}, i\epsilon) = \frac{i\epsilon - (v + \delta v)\mathbf{p}\Sigma}{1 + \delta Z}, \quad (10)$$

where  $\delta Z$  is chosen to preserve the coefficient at  $i\epsilon$  upon rescaling of the electronic fields,  $\psi \rightarrow (1 + \delta Z/2)\psi$ :  $\delta Z = \partial\Sigma(\mathbf{p}, i\epsilon)/\partial(i\epsilon)$ . Then  $v$  is renormalized as

$$\frac{\delta v}{v} = \frac{\partial\Sigma(\mathbf{p}, i\epsilon)}{\partial(i\epsilon)} + \frac{\partial\Sigma(\mathbf{p}, i\epsilon)}{\partial(v\mathbf{p}\Sigma)}. \quad (11)$$

Next, we determine renormalization of the coupling constants. The electron charge  $e$  is not changed, as guaranteed by the gauge invariance, so the renormalization of the Coulomb coupling constant  $g$  is determined by the velocity  $v$ . For the EPC, logarithmic vertex corrections of the order  $O(1/\mathcal{N}, \lambda_{\mu}^2)$  are shown in Fig. 4. Two other diagrams (Fig. 5) should be taken into account, as they are of the same order and also logarithmic. As a result,

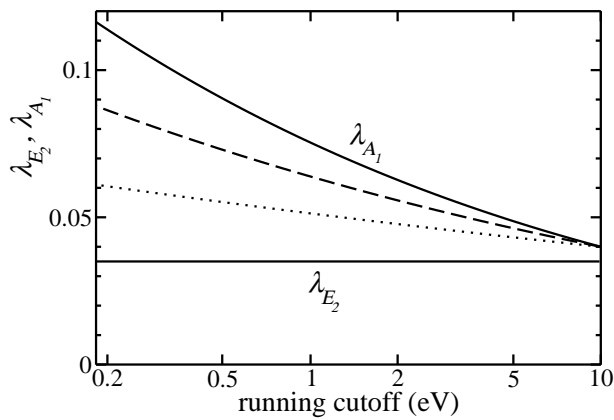


FIG. 6: Flow of the dimensionless coupling constants  $\lambda_{A_1}$  (three upper curves, starting from the bare value 0.04 at 10 eV, respectively) for three values of the bare Coulomb coupling  $g(0) = 3.4, 1.5, 0.5$  (solid, dashed, and dotted curves). The constant  $\lambda_{E_2} = 0.035$  is unchanged in the order  $O(\lambda)$ .

we obtain the following RG equations:

$$\frac{dg}{d\ell} = -\frac{8f(g)}{\pi^2\mathcal{N}}g + \frac{\lambda_{E_2} + \lambda_{A_1}}{2\pi}g, \quad (12a)$$

$$\frac{d\lambda_{E_2}}{d\ell} = \frac{\lambda_{A_1}^2}{2\pi}, \quad (12b)$$

$$\frac{d\lambda_{A_1}}{d\ell} = \frac{16f(g)}{\pi^2\mathcal{N}}\lambda_{A_1}. \quad (12c)$$

Because of the diagrams of Fig. 5, the renormalized  $\lambda_\mu$  cannot be related to a new EPC vertex  $F_\mu$ . Iterations of these diagrams generate electron coupling to multi-phonon excitations, all included in the renormalized  $\lambda_\mu$ .

The coupling constant  $\lambda_{E_2}$  at energies  $\sim \omega_{E_2} \approx 0.2$  eV can be extracted from the experimental data of Ref. [5] (change of the Raman  $G$  peak with the electron density):  $\lambda_{E_2} \approx 0.035$ , corresponding to  $F_{E_2} = 6$  eV/Å. Then the main effect comes from the Coulomb terms: as  $f(g) > 0$ ,  $g$  flows to weak coupling [15],  $\lambda_{A_1}$  is enhanced, while the enhancement of  $\lambda_{E_2}$ , proportional to  $\lambda_{A_1}^2$ , is much weaker. This behavior is in qualitative agreement with the Raman data: when the  $\lambda_\mu^2$  term is neglected, the ratio of the intensities of the two-phonon peaks, mentioned in the introduction, is  $I_{D^*}/I_{G^*} = 2(\lambda_{A_1}/\lambda_{E_2})^2$  [12]. If only Coulomb terms are kept in Eqs. (12), their integration gives  $\lambda_{A_1}(\ell)/\lambda_{A_1}(0) = [g(0)/g(\ell)]^2 = [v(\ell)/v(0)]^2$ , which, in principle, can be checked experimentally.

To study the behavior of the coupling constants quantitatively, we solve Eqs. (12) numerically, neglecting the  $\lambda_\mu^2$  term. The largest value of  $\ell$  is determined by the lower cutoff  $\xi_{min} \sim \omega_\mu \sim 0.2$  eV. In Fig. 6, we show the flow of  $\lambda_{A_1}$  for three values of the bare Coulomb coupling constant:  $g(0) = 3.4$  (corresponding to no dielectric screening at all),  $g(0) = 1.5$ , and  $g(0) = 0.5$ . The bare values of the the electron-phonon coupling constants  $\lambda_{E_2}(0) = 0.035$ ,  $\lambda_{A_1}(0) = 0.040$  were chosen (a) to satisfy the relation  $\lambda_{E_2}(0)/\lambda_{A_1}(0) = \omega_{A_1}/\omega_{E_2}$ , valid in the

tight-binding approximation, (b) to reproduce the experimental value  $\lambda_{E_2} \approx 0.035$ . For electronic energies  $\epsilon \sim 1$  eV, involved in the Raman scattering, in the totally unscreened case,  $g(0) = 3.4$ , we obtain  $\lambda_{A_1}/\lambda_{E_2} \approx 3.2$ , in agreement with the observed ratio  $I_{D^*}/I_{G^*} \approx 20$ .

*Conclusions.*— In this paper we have considered mutual effect of the weak electron-phonon and strong Coulomb interactions on each other by summing up leading logarithmic corrections via the renormalization group approach in the intermediate energy range  $\omega_{E_2}, \omega_{A_1} < \epsilon < v/a$ . At these energies quantum fluctuations of the phonon field may be viewed as effective static disorder. We find that Coulomb interaction enhances electron coupling to the intervalley  $A_1$  optical phonons, but not to the intervalley  $E_2$  phonons, in agreement with the experimental data for two-phonon Raman scattering.

We thank M. S. Foster and F. Guinea for discussions.

\* Electronic address: basko@sissa.it

- [1] A. C. Ferrari *et al.*, Phys. Rev. Lett. **97**, 187401 (2006).
- [2] A. Gupta *et al.*, arXiv: cond-mat/0606593.
- [3] D. Graf *et al.*, Nano Lett. **7**, 238 (2007).
- [4] S. Pisana *et al.*, Nature Materials **6**, 198 (2007).
- [5] J. Yan *et al.*, Phys. Rev. Lett. **98** 166802 (2007).
- [6] A. Bostwick *et al.*, Nature Physics **3**, 36 (2007).
- [7] M. Lazzeri and F. Mauri, Phys. Rev. Lett. **97**, 266407 (2006).
- [8] M. Calandra and F. Mauri, arXiv: 0707.1467.
- [9] C.-H. Park *et al.*, arXiv: 0707.1666.
- [10] D. M. Ceperley and B. J. Alder, Phys. Rev. Lett. **45**, 566 (1980); J. P. Perdew and A. Zunger, Phys. Rev. B **23**, 5048 (1981).
- [11] D. C. Langreth and M. J. Mehl, Phys. Rev. B **28**, 1809 (1983); A. D. Becke, Phys. Rev. A **38**, 3098 (1988); J. P. Perdew, K. Burke, and M. Ernzerhof, Phys. Rev. Lett. **77**, 3865 (1996).
- [12] D. M. Basko, Phys. Rev. B **76**, 081405(R) (2007).
- [13] A. A. Abrikosov and S. D. Beneslavskii, Zh. Eksp. Teor. Fiz **59**, 1280 (1970) [Sov. Phys. JETP **32**, 699 (1971)].
- [14] J. González, F. Guinea, and M. A. H. Vozmediano, Mod. Phys. Lett. B **7**, 1593 (1994); Nucl. Phys. B **424**, 595 (1994); J. Low Temp. Phys. **99**, 287 (1994).
- [15] J. González, F. Guinea, and M. A. H. Vozmediano, Phys. Rev. B **59**, R2474 (1999).
- [16] I. L. Aleiner, D. E. Kharzeev, and A. M. Tsvelik, arXiv: 0708.0394.
- [17] J. Ye, Phys. Rev. B **60**, 8290 (2005).
- [18] T. Stauber, F. Guinea, and M. A. H. Vozmediano, Phys. Rev. B **71**, 041406(R) (2005).
- [19] M. S. Foster and I. L. Aleiner (to be published).
- [20] P. R. Wallace, Phys. Rev. **71**, 622 (1947).
- [21] E. McCann *et al.*, Phys. Rev. Lett. **97**, 146805 (2006).
- [22] I. L. Aleiner and K. B. Efetov, Phys. Rev. Lett. **97**, 236801 (2006).
- [23] S. Piscanec *et al.*, Phys. Rev. Lett. **93**, 185503 (2004).
- [24]  $\Sigma^{ph}$  in graphite was considered long ago [F. Guinea, J. Phys. C: Solid State Phys. **14**, 3345 (1981)], but the logarithmic divergence was not noted in that work.

- [25] J. Maultzsch, S. Reich, C. Thomsen, H. Requardt, and P. Ordejón, Phys. Rev. Lett. **92**, 075501 (2004).